



Femtosecond laser irradiation of titanium oxide thin films: accumulation effect under IR beam

A. Talbi¹ · N. Semmar¹ · M. Tabbal² · G. O' Connor³ · P. Coddet¹ · A.-L. Thomann¹ · A. Stolz¹ · C. Leborgne¹ · E. Millon¹

Received: 4 February 2020 / Accepted: 18 April 2020 / Published online: 4 May 2020
© Springer-Verlag GmbH Germany, part of Springer Nature 2020

Abstract

This paper discusses the mechanisms of laser-induced periodic surface structures (LIPSS) formation using a high repetition rate femtosecond laser beam irradiation of magnetron-sputtered titanium oxide thin films ($\text{TiO}_{1.8}$) grown onto SiO_2/Si substrates. An Yb:YKW 500 fs linearly polarized laser emitting at a wavelength, λ , of 1030 nm, was used to irradiate the films (300 nm thickness) at a repetition rate of 100 kHz under both static and dynamic (scanning) conditions. Under static beam conditions, an incubation behavior related to materials in thin film form was established with a damage threshold of 72 mJ/cm^2 . Close to this fluence value and increasing the number of laser shots from 1 to 1000, micro-cracking occurred and propagated inside the beam waist diameter zone estimated close to $60 \mu\text{m}$. In addition, using a higher fluence value of 280 mJ/cm^2 , i.e., well above the damage threshold, a melting occurred in an intermediate zone within the irradiated area, with a surprising 'cure effect' that contributes to the micro-cracks stabilization. Simultaneously, at the center of the Gaussian laser beam spot, the entire film ablation was observed. Furthermore, irradiation under dynamic mode with a scanning speed of 4 mm/s and a repetition rate of 100 kHz were achieved for the large-scale processing of the $\text{TiO}_{1.8}$ films up to surface area of $25 \times 25 \text{ mm}^2$. For these irradiation conditions case that correspond to a fluence of 110 mJ/cm^2 and a cumulative number of shots of 3000, 2D-LIPSS nano-cracks (200 nm length and $\lambda/8$ to $\lambda/9$ period) are obtained over the whole irradiated surface, a phenomenon that is mainly attributed to a thermo-mechanical ablation mechanism.

Keywords Titanium oxide film · Femtosecond laser beam · High repetition rate · LIPSS · Incubation · Micro/nano-cracks

1 Introduction

The investigation of laser-induced periodic surface structures (LIPSS) has found renewed interest when it was shown that femtosecond lasers offer the possibility to induce structures with periods significantly smaller than the irradiation wavelength, the so-called high spatial frequency LIPSS (HSFL) [1–3]. As opposed to the commonly obtained low spatial frequency LIPSS (LSFL) [4, 5], whose period is

close to the irradiating beam wavelength, HSFL formation calls for a new understanding of the underlying physical phenomena and could pave the way for novel applications in tribology, cell growth, optical data storage and encryption as well as the fabrication of hydrophobic surfaces [6–10]. Most of these applications will require homogeneous LIPSS generation over large areas obtained by scanning a focused laser beam on the material surface using high repetition rate lasers (100 kHz or more). In some instances, the treated material, which can be a metal [11], a semiconductor [12] or a dielectric [13], is in thin film form. Despite the great attention paid to the study of the physical mechanisms leading to the formation of LIPSS using femtosecond lasers, the existing models are still a matter of investigation because of the complex processes involved during the ultrashort laser-matter interaction. While the experimental results observed with bulk materials are generally in good agreement with theoretical models such as the interference model including the excitation of surface plasmon polaritons, the self-organization model and hydrodynamic approaches [14–17];

✉ E. Millon
eric.millon@univ-orleans.fr

¹ GREMI, UMR 7344 CNRS / Université D'Orléans, 14 rue d'Issoudun, B.P. 6744, 45067 Orléans Cedex 2, France

² Department of Physics, American University of Beirut, Bliss St, P.O. Box 11-0236, Riad el Solh, Beirut 1107 2020, Lebanon

³ NCLA/Inspire Laboratories, School of Physics, National University of Ireland Galway, University Road, Galway, Ireland

however, in the case of thin films, additional physical effects have to be taken into account such as cavitation bubbles, delamination, substrate effect, thin film adhesion and thermo-elastic stresses [18, 19]. These effects may induce complex phenomena to occur during laser radiation that can yield to a unusual and exotic surface organization structures that are specific to thin films [20].

The formation of LIPSS on titanium oxide (TiO_x) thin films has been the subject of recent research owing to the high technological importance of TiO_x in the energy and environmental fields [21, 22]. Recent results from our group indicate that a wide variety of LIPSS patterns and morphologies can be obtained on TiO_x films by careful tuning of the irradiation parameters such as laser fluence and laser scanning parameters [23]. However, most of these results were obtained at repetition rates of 1 kHz and using pulsed laser-deposited (PLD) TiO_x films, which makes the scale-up of LIPSS formation to large areas a tedious and difficult process. Furthermore, a comparative study between LIPSS generated on PLD TiO_x and those obtained on magnetron-sputtered TiO_x films (a large-scale compatible deposition technique) evidenced similarities except for delamination and cracking that only appeared on the latter films [24]. This differing behavior is expected to be related to the difference in thermo-mechanical properties [24–27] of the films. Thus, the present work focuses on the investigation of LIPSS formation on the surface of magnetron-sputtered titanium oxide thin films following irradiation with a femtosecond laser at 100 kHz, thereby making the process scalable to large areas. Emphasis is placed on the study of complex organization mechanisms of the surface patterns that appear particular to materials in thin film form.

2 Experimental details

Magnetron sputtering (MS) was used to grow titanium oxide thin films with typical thicknesses ranging between 300 and 500 nm onto 1.2 μm thick SiO_2 layers thermally grown on Si (100) substrates (Fig. 1). A 10-cm diameter and 4.0-mm-thick titanium metallic target (purity 99.995%) was sputtered in a pulsed DC mode using a mixture of Ar and O_2 gas. Details of the sputtering system are available elsewhere [23, 24, 28]. Film growth was achieved on an unheated rotating substrate holder placed at a distance of ~ 127 mm from the target at a total pressure of 1 Pa (base pressure of $\sim 10^{-5}$ Pa). The flow rates of argon and oxygen were fixed at 20 and 1.5 sccm, respectively. Under these conditions, homogenous (over an area of $5 \times 5 \text{ cm}^2$) titanium oxide thin films with an O/Ti ratio of 1.8, as measured by Rutherford backscattering spectrometry (RBS), were obtained. Typically, in the growth conditions used in the present work, the film micro-structure is expected to be amorphous-like, since no post-deposition annealing was performed. In addition, the scanning electron microscope (SEM) images (Fig. 1) obtained for these films indicate a columnar-like growth of titanium oxide with an average surface roughness (estimated from the SEM cross section seen in Fig. 1) to be lower than 10 nm. Such surface topology would have little effect on the LIPSS formation since LIPSS dimensions (width and period) are in the range of several hundred of nm, as discussed later in this work.

Laser irradiation experiments were performed on the films using a Yb:YKW 500 fs linearly polarized laser emitting at 1030 nm that can operate at a repetition rate up to 300 kHz. The details of the irradiation set-up are similar to those presented elsewhere [23, 24, 29]. Briefly, the laser beam is focused onto the surface of the thin film using a galvanometer scanner with an F-theta lens having a focal distance of 100 mm. Samples were irradiated in static mode (single-spot irradiation with different numbers of pulses) and in dynamic mode (large-area irradiation by laser scanning).

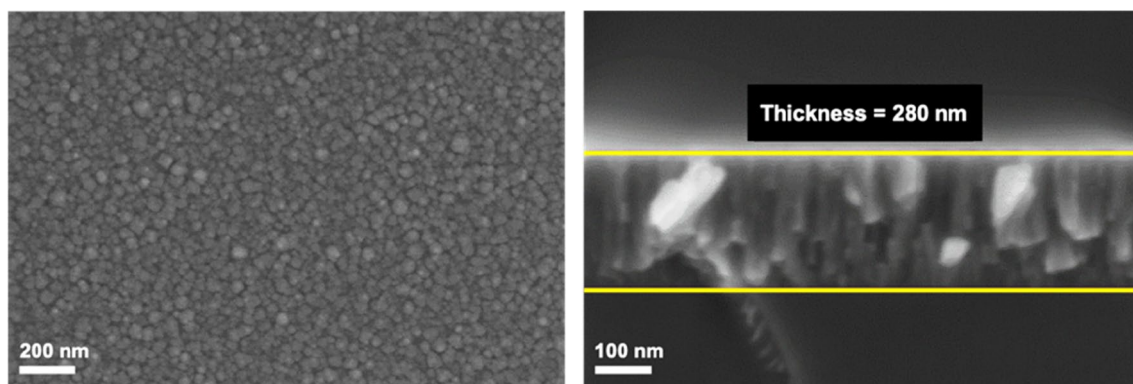


Fig. 1 SEM top and cross section views of the MS deposited TiO_x thin film. The thickness is about 280 nm

In the latter mode, treatment of large surfaces was accomplished by fixing the samples on the X – Y translation device, and a mirror reflecting the laser beam onto the sample. The operating conditions are then controlled by the mean number of laser pulses when adjusting the translation step (S) in the Y direction for a scan speed of 4 mm/s in the X direction. The laser repetition rate is fixed at 100 kHz. The beam waist radius, in this case, was determined to be 32 μm , using the Liu method [30] under static irradiation mode, as described in the results section. The laser impact and surface morphology of the irradiated films were investigated using an Olympus SZ61 optical stereo microscope and a Zeiss SUPRA 40 high resolution field emission scanning electron microscope.

3 Results

Figure 2 shows optical microscopy images of the laser spot obtained on $\text{TiO}_{1.8}$ thin films irradiated at different energies, E , and for different values of the number of pulses N . The beam energy and the number of pulses were varied, respectively, in the range of 1.25 to 16 μJ (values measured with a power meter just before the galvanometer scanner) and 1 to 100,000 pulses. The determination of damage threshold fluence was

performed according to Liu's method [30], which consists in varying the beam energy at a fixed focal spot (the target-lens distance is unvaried). No laser crater was observed on the films irradiated at 2 μJ and N ranging between 1 and 1000, nor for irradiation at 3 μJ and 1 pulse. Images corresponding to these latter conditions have thus been omitted from Fig. 2.

The ablation threshold is commonly defined as the laser fluence at which a surface modification, induced by an ablation process. Otherwise, if the ablation process does not clearly take place, the measured threshold corresponds to the surface damage threshold (which can be attributed to thin film specific processes: melting, cavitation, cracking (stress) and delamination). The ablation threshold for our $\text{TiO}_{1.8}$ films is determined from the images of Fig. 2 as follows. The crater diameter of each spot was measured and plotted versus the laser fluence used to ablate the film and form the crater. The threshold was deduced from Eq. 1, which describes the relationship between the laser fluence F , and the crater diameter D [30].

$$D^2 = 2\omega_0^2 \ln \left(\frac{F}{F_{\text{th}}} \right) \quad (1)$$

where ω_0 refers to the beam waist radius parameter (measured at $1/e$). The beam waist can be estimated from the slope

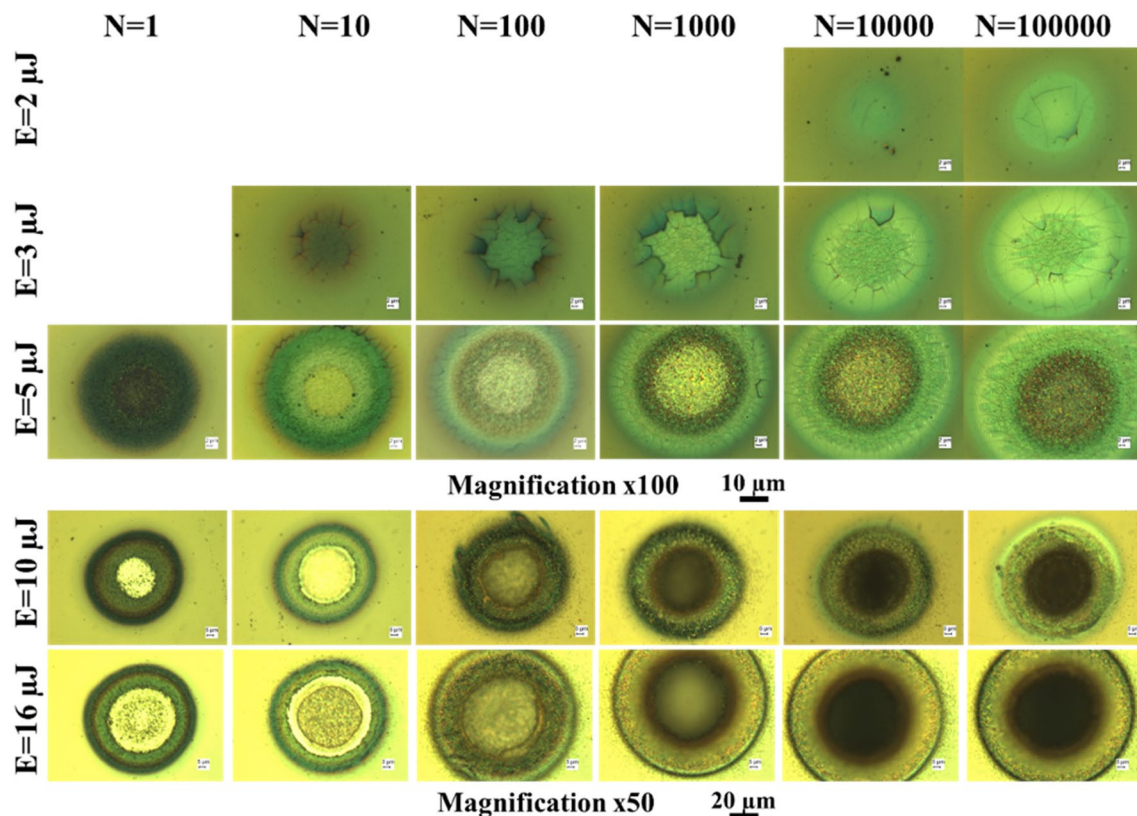


Fig. 2 Optical microscopy characterization of laser spot formed on $\text{TiO}_{1.8}$ thin films irradiated by 500 fs laser at 1030 nm for different energies E and number of pulses N

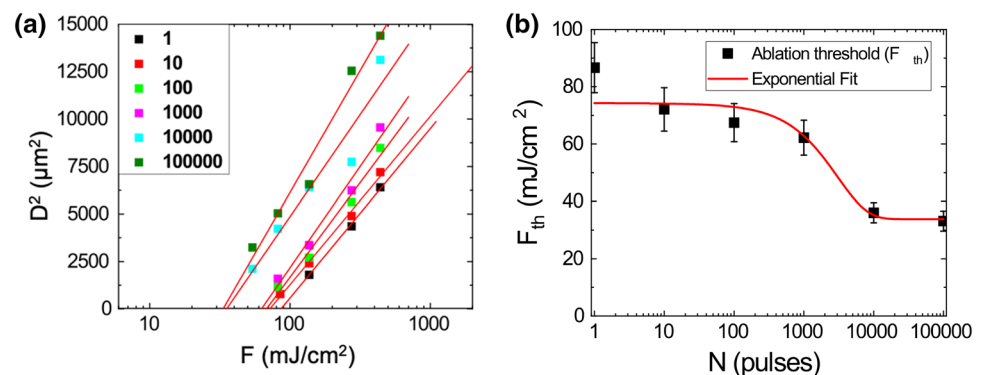
of the linear curves obtained through a semi-log plot of D^2 as a function of the fluence. Such curves are displayed in Fig. 3 (a) for different values of the number of pulses, N , and the beam waist radius was found to be about $32\ \mu\text{m}$. The ablation thresholds for different values of N were determined from the intercepts with the x-axis of the D^2 versus $\ln(F)$ curves. A semi-log plot of the threshold of ablation fluence (F_{th}) as a function of N is shown in Fig. 3 (b). The latter figure shows that the damage threshold fluence is determined close to $80\ \text{mJ}/\text{cm}^2$ for a single pulse, and it decreases monotonously with increasing pulse number, reaching $62\ \text{mJ}/\text{cm}^2$ for 1000 pulses. A further increase in the number of pulses to 10,000 leads to a sharp decrease down to $36\ \text{mJ}/\text{cm}^2$, the value at which the curve appears to saturate as a further increase in the number of pulses (up to 100,000) results in only a slight decrease to $33\ \text{mJ}/\text{cm}^2$. The decrease in the ablation threshold fluence with increasing number of pulses is a well-known phenomenon in the case of metals and semiconductors (such as Si) and typically follows an exponential decrease. For these materials, this so-called ‘incubation effect’ is attributed to the accumulation of defects (such as oxidation, stress, dislocations) that are generated and increased pulse by pulse. In the case of insulators, incubation behavior appears more complex due to the non-linear processes that govern the first stage of pulse absorption. This is indeed the case in this work, as Fig. 3 (b) cannot be modeled by an exponential decrease. In fact, the variation of $F_{\text{th}}(N)$ as a function of N can be characterized by two regimes, in agreement with results reported in the literature for dielectric thin films such as HfO_2 , Sc_2O_3 , Ta_2O_5 , Al_2O_3 and SiO_2 [11, 31–34]. The first regime shows a decrease in the fluence threshold (ablation and damage) as a function of the number of pulses, while the second one exhibits a saturation step (also called stabilization). This is observed in our case at a number of pulses of 10,000, with the saturation value of the fluence referred to as $F_{\text{th}}(\infty)$, reflecting the minimum fluence needed to induce damage on the films surface. The ratio of this value to the single-pulse threshold ($F_{\text{th}}(\infty)/F_{\text{th}}(1)$) typically ranges between 0.1 to 0.9 for dielectric oxide films [35]. In our case, with

$F_{\text{th}}(1) \sim 72\ \text{mJ}/\text{cm}^2$ and $F_{\text{th}}(\infty) \sim 36\ \text{mJ}/\text{cm}^2$, leading to a value of the ratio $F_{\text{th}}(\infty)/F_{\text{th}}(1)$ close to 0.2.

In order to investigate the nature of surface damage, SEM observations of the laser spots were performed on the irradiated samples. Figure 4 shows the evolution of spot surface morphology with increasing N from 10 to 10,000 at a working fluence of $85\ \text{mJ}/\text{cm}^2$. For $N=10$, micro-cracks appear on the entire surface though mainly around the rim of the laser spot. For $N>100$, a similar effect is evidenced, with clear film delamination that appears more pronounced around the rim of the laser spot. It is widely accepted that the cracking, fragmentation and delamination of material occurs due to the thermo-elastic stresses induced by laser irradiation [32]. As a result of the sub-picosecond pulse (500 fs), the laser energy absorption causes a confined heat in the irradiated volume. This thermal confinement leads to an increase in the temperature of the irradiated zone, generating thermoelastic stresses [33]. Due to the repeated rapid heating/cooling process, a very high density of thermoelastic stresses is generated, which causes a fracture by fatigue and delamination of the thin film. The images shown in Fig. 4 also suggest that the induced damage threshold measured above is not based on evaporation/melting but rather on cracking and delamination.

Further investigation of the damage processes occurring under static irradiation was achieved by varying the laser fluence at values above the damage threshold while keeping the number of pulses fixed. Figure 5 shows SEM images of three laser spots formed after 10 pulses for three different fluence values, namely 85 , 140 and $280\ \text{mJ}/\text{cm}^2$ (all above the $72\ \text{mJ}/\text{cm}^2$ damage threshold value determined for this number of pulses, as reported in Fig. 3). For a fluence of $85\ \text{mJ}/\text{cm}^2$, i.e., close to the damage threshold, some cracks are generated on the entire laser area ($28\ \mu\text{m}$ in diameter). When F is increased up to $140\ \text{mJ}/\text{cm}^2$, the central zone ($18\ \mu\text{m}$) appears as a melted region with the presence of a few cracks. Around this zone, more pronounced cracks develop (rim zone). Lastly, for a relatively high fluence of $280\ \text{mJ}/\text{cm}^2$, three types of damage can be distinguished on a laser area of $75\ \mu\text{m}$. This is clearly related to the Gaussian

Fig. 3 **a** Semi-log plots of laser spot square diameter D^2 versus laser fluence F . **b** Evolution of threshold ablation fluence F_{th} of $\text{TiO}_{1.8}$ thin film versus number of pulses N for a 500 fs laser at 1030 nm



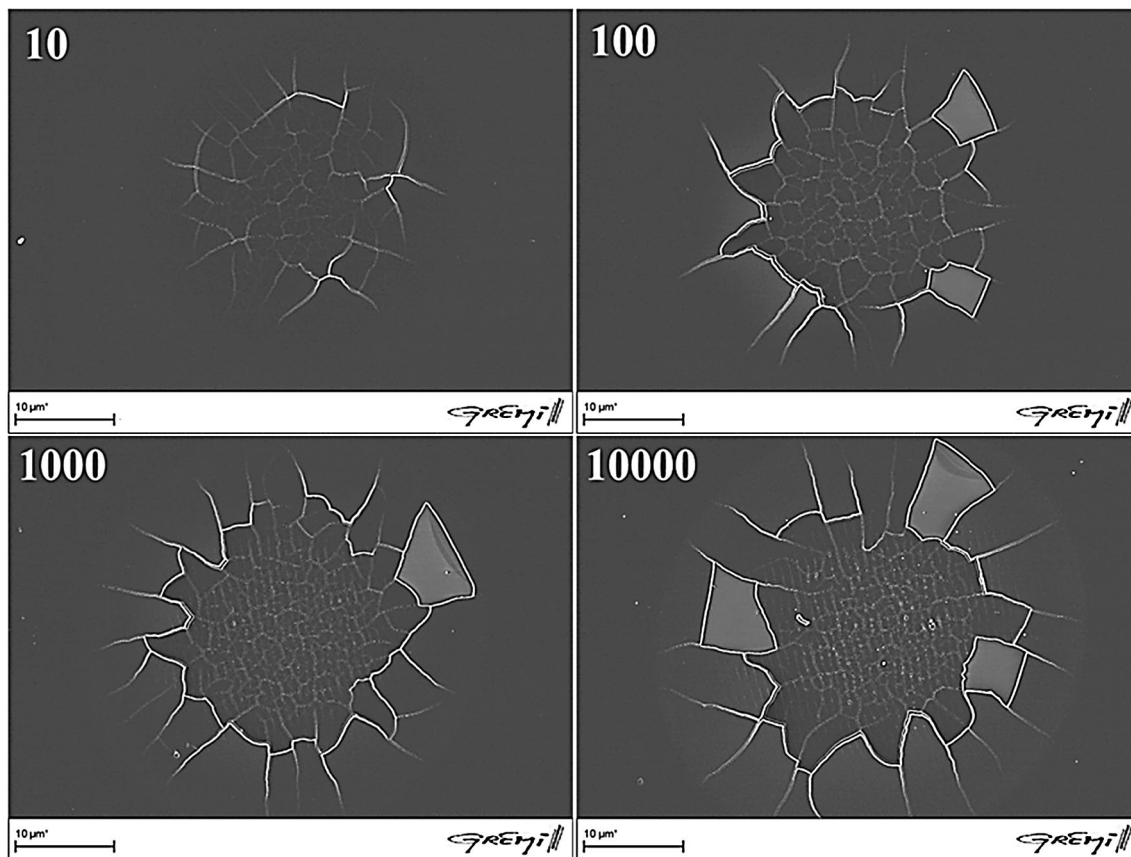


Fig. 4 SEM views of laser spots formed on TiO_{1.8} thin film under 500 fs laser irradiation at 1030 nm. The fluence was fixed at 85 mJ/cm² and *N* was varied from 10 to 10,000

profile of the laser beam used in this study. In the center, where the laser energy density is the highest, the film is severely ablated. Moving radially away from this zone, the energy density decreases and a clear melted ring can be observed. Further away, in the outer regions, the energy density is even lower and cracks are still formed. Therefore, it is evident that the fluence threshold is the highest for the ablation-like process, the lowest for cracking and intermediate for melting. A sketch of the Gaussian beam effect is shown in Fig. 6, along with three threshold fluences that are matched to the different damage locations for a sample irradiated at 280 mJ/cm².

As reported in our previous work on titanium oxide films [24], large surface area laser processing induces several morphological changes depending on the accumulated laser dose and on the scanning parameters. To link the following section, in which we present results under dynamic (scanning) mode irradiation, to the previous one, it is important to evaluate the ‘equivalent’ working fluence and the corresponding number or laser shots (*Nx*). The simple formula that correlates the overlap (*Ov*) to the *X* scan speed (*Vx*), the beam diameter (*D*) and the repetition rate (*f*), returns also the number of shots as described in the following equation:

$$O_v(\%) = 100 \cdot \left(1 - \frac{V_x}{f \cdot D}\right), N_x = D \cdot \left(\frac{f}{V_x}\right) \tag{2}$$

In this work, the repetition rate, scan speed and spacing between lines were fixed to 100 kHz, 4 mm/s and 5 μm, respectively. This results in an average number of pulses of 24,000, according to Eq. 2. All the used fluences were above the surface damage threshold (36 mJ/cm² after 10,000 shots). Our observations are the following. For a fluence ranging from 55 to 85 mJ/cm², significant delamination takes place. However, for *F* higher than 110 mJ/cm², the delamination effect seems to be stabilized and a micro-cracked surface morphology is observed [24]. The surface can be damaged through two main processes: cracks and delamination induced by thermo-elastic stresses and/or ablation, evaporation and melting induced by the lattice heating due to heat accumulation. If the fluence is over the cracking (stress) threshold but below the ablation (evaporation and melting) threshold, this can lead to significant removal of the film through cracking and delamination in the form of flakes. This would correspond in our case to a fluence below 110 mJ/cm². Otherwise, if the fluence is above this melting and cracking fluence threshold but does not exceed the

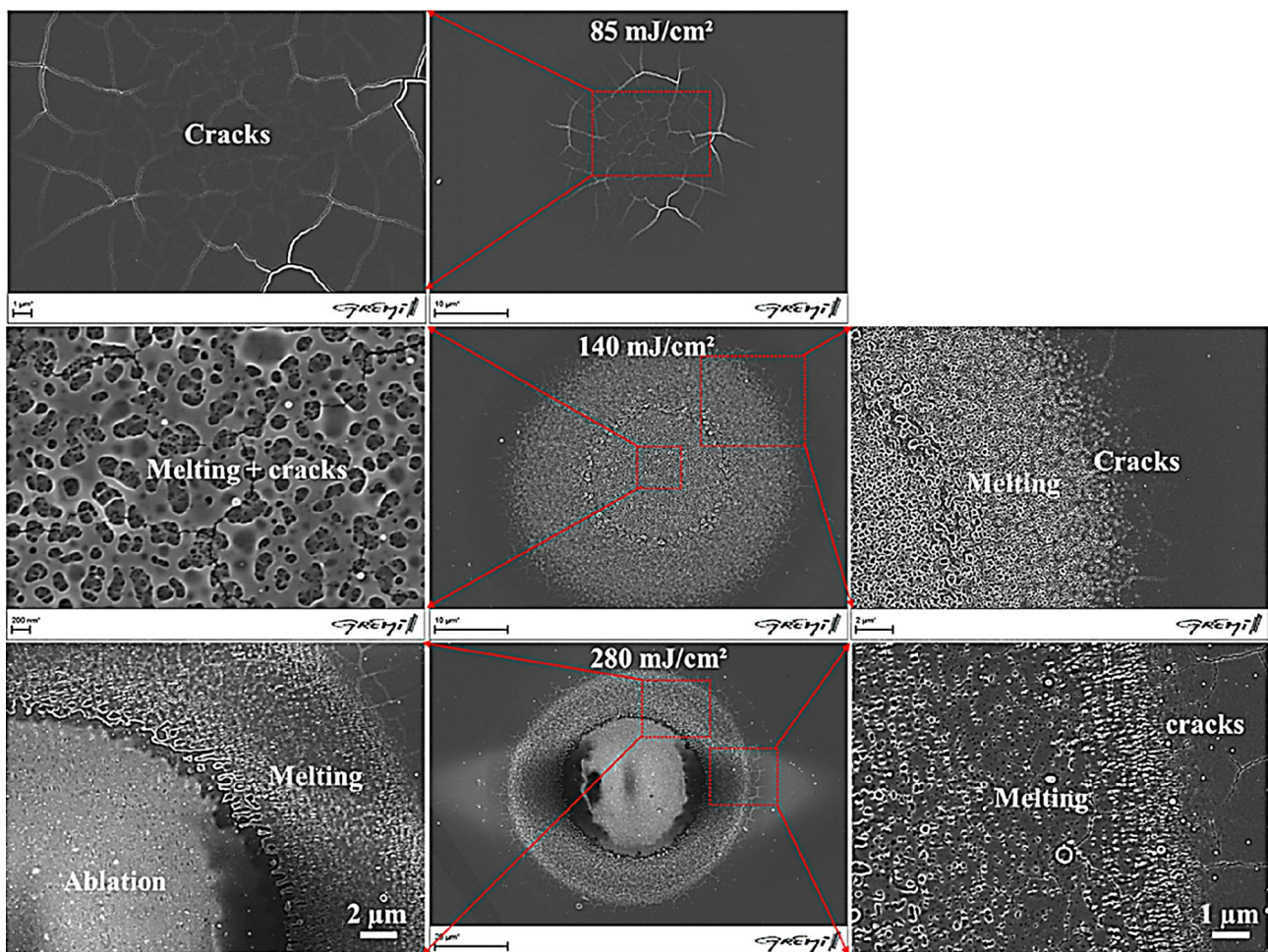


Fig. 5 SEM images of laser spot formed on $\text{TiO}_{1.8}$ thin film under 500 fs irradiation at 1030 nm after 10 pulses and at three different fluences: **a** 85 mJ/cm^2 , **b** 140 mJ/cm^2 and **c** 280 mJ/cm^2

ablation (evaporation) threshold, the laser irradiation always induces a thermo-elastic stress, which, in turn, generates cracks. However, concurrent to this mechanism, melting can take place causing stress relaxation and cracks stabilization.

SEM images of the rim region of the surface treated at 110 mJ/cm^2 are given at different magnifications in Fig. 7. On the rim of the treated zone, some highly periodic structures are observed (Fig. 7a). This organization is formed at the beginning of the laser scan, and thus, the number of pulses is expected to be lower than 24,000 pulses. About 30 μm from the rim, delamination starts to take place, producing the same morphology as that shown in our previous study [24] for $F = 110 \text{ mJ}/\text{cm}^2$. The magnified SEM image (Fig. 7b) shows the formation of highly periodic and regular vertical LIPSS with a period of about 850 nm ($\sim 0.82\lambda$) and an orientation parallel to the beam polarization. In the same image, several micro-cracks are randomly generated. In Fig. 7c, it can be seen that the LIPSS do not seem to be formed due to material transport and organization (leading

to the formation of crests and valleys or modulated surface heights), but rather as a result of the formation of nano-cracks organized in well-defined periodic localized zones (with an average period of 120 nm (in the range $\lambda/9 - \lambda/8$) and perpendicular to the beam polarization). Yet again, the thermo-elastic stress induced by beam accumulation can be considered as a possible mechanism, leading to the generation of these nano-cracks. In other words, the cracks are formed at two different scales, nano and micro-scales and produced due to the thermo-elastic stresses induced by the electromagnetic (EM) field of the laser beam. If we assume that micro- and nano-cracks are both generated as a result of stress induced by the laser, the question is why the micro-cracks are randomly generated while the nano-cracks are produced and confined to highly periodic zones. The interference model, based on Sipe's theory, may answer this question and explain LSFL organization. In general, this model predicts the formation of LIPSS as a result of non-uniform laser energy deposition. It can therefore be assumed

Fig. 6 Illustration showing the different threshold fluences for a sample irradiated at 280 mJ/cm²

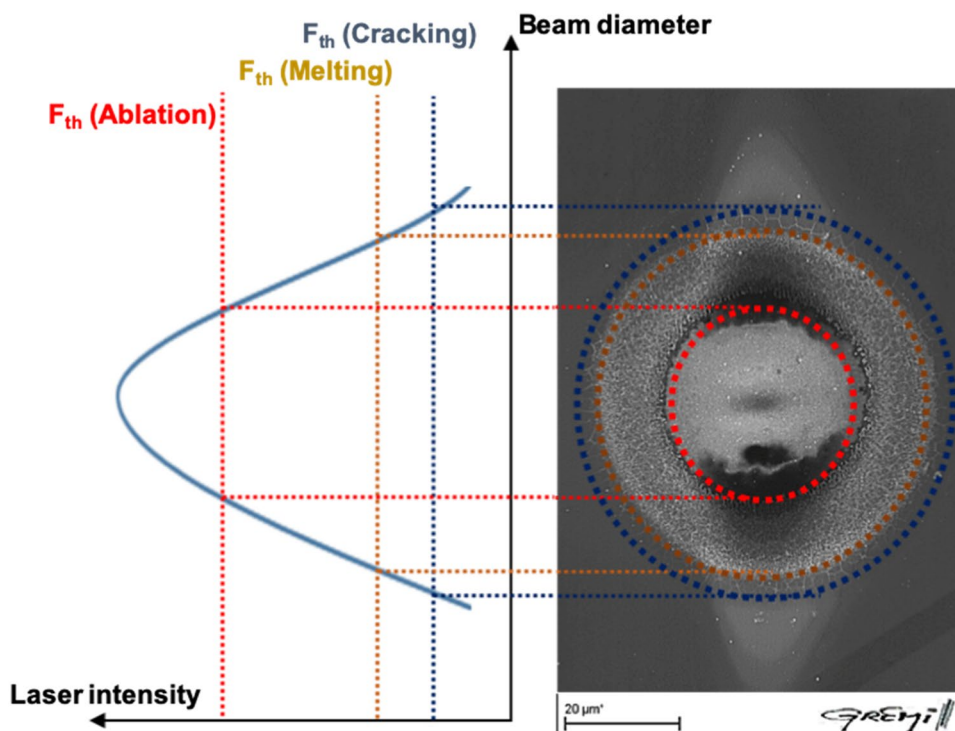
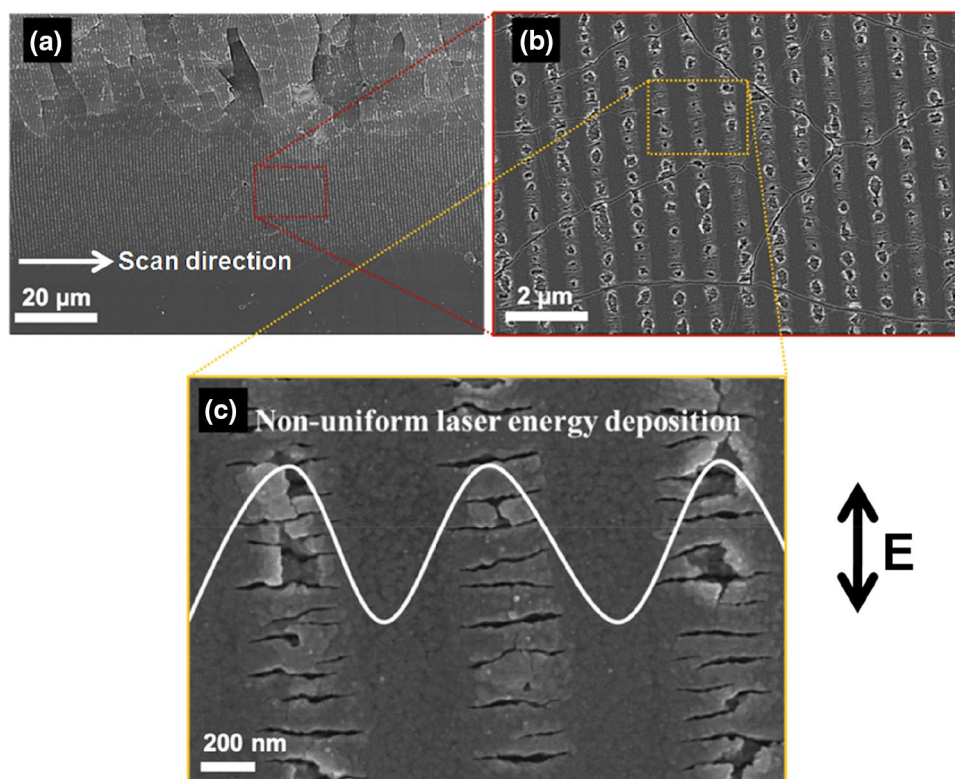


Fig. 7 SEM images characterizing the rim of large treated surface area of TiO_{1.8} at $N=24,000$ and $F=110 \text{ mJ/cm}^2$ ($S=5 \mu\text{m}$, $v=4 \text{ mm/s}$). **a** Large-scale view. **b** Zoom in the microstructures. **c** Illustration of the non-uniform laser energy deposition proposed to explain nano-crack-based LIPSS formation



that the nano-cracks LSFL regions correspond to the localized hot regions receiving the highest amount of laser energy that generates thermo-elastic stress in these regions. However, the regions located between LSFL do not receive a

large enough laser energy (i.e., higher than the local cracking threshold fluence) to generate thermo-elastic stresses. Thus, these zones remain unaffected. A schematic illustration of the non-uniform laser energy deposition that would support

this explanation is given in Fig. 7c. Another explanation that can support this interpretation is the local field enhancement [36, 37]. The first few laser pulses can be assumed to cause the formation of some tiny nano-cracks (located in the LSFL regions). These tiny nano-cracks would act as scattering centers, so that the following pulses can reinforce ionization processes due to the local field enhancement in their vicinity. This leads to the occurrence of localized high electron densities around the nano-cracks. The local field enhancement contributes to enlarging these nano-cracks in the direction perpendicular to the laser polarization. Indeed, in our case, the nano-cracks generated are found to be perpendicularly oriented to the beam polarization). This assumption was also recently suggested by Rudenko et al. [38] to explain the formation of sub-wavelength periodic nanostructures at the surface and in the bulk of glasses. In their case, nanopores and nano-voids induced by the laser were considered as the scattering centers.

Finally, we observed that nano-crack-based LSFL are formed on the rim of the irradiated area- but for the rest of the treated surface, delamination destroys these structures. However, we obtained homogenous surfaces covered by nano-crack-based LSFL at the same fluence but at a lower number of pulses down to 3000 pulses. To achieve this, the speed scan was fixed at 4 mm/s, but the spacing between lines was increased to 40 μm . Under these experimental conditions, a large surface area covered by very regular nano-cracks was formed concomitantly with random micro-cracks, as shown in Fig. 8.

4 Conclusion

The stress effect induced by the EM field of the femtosecond laser beam is evidenced in the formation of LIPSS-like nano-cracks on the $\text{TiO}_{1.8}$ magnetron-sputtered films. The “hierarchical” damage sketch suggests that, before the complete removal of the thin film, the micro-crack process starts at a low fluence, and that could be repaired and stabilized by a melting induced effect. Large surface processing of titanium oxide films with regular nano-cracks of 200 nm in size was also achieved. These kind of structures, rarely reported in the literature with such size and period, are attributed to the accumulation of mechanical stress during film sputtering and laser beam incubation effect that induce finally ablative-like HSFL.

Acknowledgements The authors gratefully acknowledge the region ‘Centre-Val-de-Loire’ and the doctoral school ‘ED-EMSTU’ for supporting this work via the ‘PIA Tours 2015’ National Project, and the PhD students’ grants. MT would like to thank the ‘University of Orleans’ and the ‘SAFAR program’ for a fellowship held during the completion of this work.

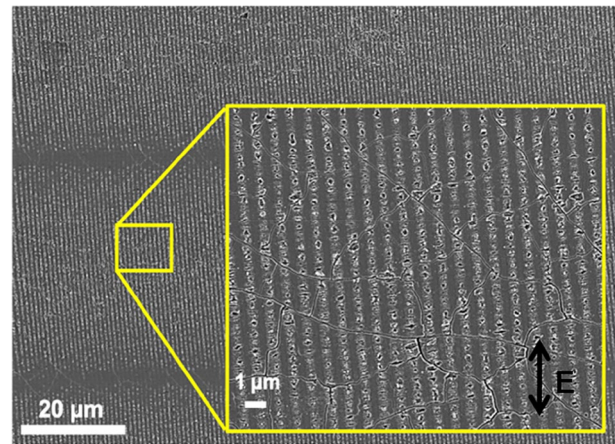


Fig. 8 SEM images of large treated surface area $\text{TiO}_{1.8}$ irradiated by 500 fs laser at 1030 nm for $N=3000$ and $F=110 \text{ mJ/cm}^2$ ($S=40 \mu\text{m}$, $v=4 \text{ mm/s}$)

References

1. S. Höhm, A. Rosenfeld, J. Krüger, J. Bonse, *J. Appl. Phys.* **112**(1), 014901 (2012). <https://doi.org/10.1063/1.4730902>
2. S. Höhm, A. Rosenfeld, J. Krüger, J. Bonse, *Appl. Surf. Sci.* **278**, 7–12 (2013). <https://doi.org/10.1016/j.apsusc.2012.10.188>
3. A.V.D. Ostovalov, V.P.K. Orolkov, K.A.O. Kotrub, B. Ronnikov, S.A.B. Abin, *Op. Ex.* **26**(6), 7712–7723 (2018). <https://doi.org/10.1364/OE.26.007712>
4. T.J.Y. Derrien, R. Koter, J. Krüger, S. Hohm, A. Rosenfeld, J. Bonse, *J. Appl. Phys.* **116**, 074902 (2014). <https://doi.org/10.1063/1.4887808>
5. T.T.D. Huynh, A. Petit, N. Semmar, *App. Surf. Sci.* **302**, 109–113 (2014). <https://doi.org/10.1016/j.apsusc.2013.10.172>
6. F.A. Müller, C. Kunz, S. Gräf, *Materials* **9**, 476 (2016). <https://doi.org/10.3390/ma9060476>
7. A.Y. Vorobyev, C. Guo, *Laser Photon. Rev.* **7**(3), 385–407 (2013). <https://doi.org/10.1002/lpor.201200017>
8. A.H.A. Lutey, L. Gemini, L. Romoli, G. Lazzini, F. Fuso, M. Facon, R. Kling, *Sci. Rep.* **8**, 10112 (2018). <https://doi.org/10.1038/s41598-018-28454-2>
9. B. Öktem, I. Pavlov, S. Ilday, H. Kalaycıoğlu, A. Rybak, S. Yavaş, M. Erdoğan, F. Ömer Ilday, *Nature. Photon.* **7**, 897–901 (2013). <https://doi.org/10.1038/nphoton.2013.272>
10. A.G. Kovačević, S. Petrović, V. Lazović, D. Peruško, D. Pantelić, B.M. Jelenković, *App. Surf. Sci.* **417**, 155–159 (2017). <https://doi.org/10.1016/j.apsusc.2017.03.141>
11. G. Raciukaitis, M. Brikas, P. Geceys, M. Gedvilas, *Proceedings of SPIE Conference on High-Power Laser Ablation VII 7005, 70052L* (2008). <https://doi.org/10.1117/12.782937>
12. A. Borowiec, H.K. Haugen, *Appl. Phys. Lett.* **82**(25), 4462–4464 (2003). <https://doi.org/10.1063/1.1586457>
13. F. Costache, M. Henyk, J. Reif, *Appl. Surf. Sci.* **186**(1–4), 352–357 (2002). [https://doi.org/10.1016/S0169-4332\(01\)00675-4](https://doi.org/10.1016/S0169-4332(01)00675-4)
14. G.D. Tsididis, M. Barberoglou, P.A. Loukakos, E. Stratakis, C. Fotakis, *Phys. Rev. B* **86**, 115316 (2012). <https://doi.org/10.1103/PhysRevB.86.115316>
15. M. Straub, M. Afshar, D. Feili, H. Seidel, K. König, *J. Appl. Phys.* **111**, 124315 (2012). <https://doi.org/10.1063/1.4730381>
16. J.F. Young, J.S. Preston, H.M. Van Driel, J.E. Sipe, *Phys. Rev. B* **27**, 1155–1172 (1983). <https://doi.org/10.1103/PhysRevB.27.1155>

17. O. Varlamova, J. Reif, S. Varlamov, M. Bestehorn, 2015 in *Progress in Nonlinear Nano-Optics. Nano-Optics and Nanophotonics*, ed. by S. Sakabe, C. Lienau, R. Grunwald (Springer, Berlin). doi 10.1007/978-3-319-12217-5_1
18. D. Scorticati, G.-W.R.B.E. Römer, D.F. de Lange, B. Huis in't Veld, J. Nanophotonics **6**(1), 063528 (2012). <https://doi.org/10.1117/1.JNP.6.063528>
19. Z. Zhou, W. Ma, Thin Solid Films **519**(22), 7940–7946 (2011). <https://doi.org/10.1016/j.tsf.2011.05.062>
20. T.T.D. Huynh, N. Semmar, Appl. Phys. A **116**, 1429–1435 (2014). <https://doi.org/10.1007/s00339-014-8255-0>
21. A. Fujishima, X. Zhang, D.A. Tryk, Surf. Sci. Rep. **63**(12), 515–582 (2008). <https://doi.org/10.1016/j.surfrep.2008.10.001>
22. I. Vaiciulis, M. Girtan, A. Stanculescu, L. Leontie, F. Habelhames, S. Antohe, Proc. Rom. Acad. Ser. A **13**(4), 335–342 (2012)
23. A. Talbi, C. Tchiffo-Tameko, A. Stolz, E. Millon, C. Boulmer-Leborgne, N. Semmar, Appl. Surf. Sci. **418B**, 425–429 (2017). <https://doi.org/10.1016/j.apsusc.2017.02.033>
24. A. Talbi, P. Coddet, M. Tabbal, A.-L. Thomann, E. Millon, A. Stolz, C. Boulmer-Leborgne, G.M. O'Connor, N. Semmar, Appl. Surf. Sci. **476**, 303–307 (2019). <https://doi.org/10.1016/j.apsusc.2019.01.069>
25. C. McDonnell, D. Milne, C. Prieto, H. Chan, D. Rostohar, G.M. O'Connor, Appl. Surf. Sci. **359**, 567–575 (2015). <https://doi.org/10.1016/j.apsusc.2015.10.019>
26. R. Benocci, D. Batani, H.E. Roman, Appl. Phys. B **125**, 22 (2010). <https://doi.org/10.1007/s00340-019-7132-0>
27. F. Kiel, N.M. Bulkakova, A. Ostendorf, E.L. Gurevich, Phys. Rev. Applied **11**, 024038 (2019). <https://doi.org/10.1103/PhysRevApplied.11.024038>
28. P.-A. Cormier, A. Balhamri, A.-L. Thomann, R. Dussart, N. Semmar, T. Lecas, R. Snyders, S. Konstantinidis, Surf. Coat. Technol. **254**, 291–297 (2014). <https://doi.org/10.1016/j.surfcoat.2014.06.037>
29. A. Talbi, Ph.D. thesis, University of Orleans (2017), <https://tel.archives-ouvertes.fr/tel-01952834/document>
30. J.M. Liu, Opt. Lett. **7**(5), 196–198 (1982). <https://doi.org/10.1364/OL.7.000196>
31. D. Douti, L. Gallais, M. Commandré, Opt. Eng. **53**(12), 122509 (2014). <https://doi.org/10.1117/1.OE.53.12.122509>
32. D. N. Nguyen, L. A. Emmert, M. Mero, W. Rudolph, Proceedings of SPIE Conference on Laser-Induced Damage in Optical Materials 7132, 71320N (2008). <http://dx.doi.org/10.1117/12.804452>
33. M. Mero, B.R. Clapp, J.C. Jasapara, W.G. Rudolph, D. Ristau, K. Starke, J. Krüger, S. Martin, W. Kautek, Opt. Eng. **44**(5), 051107 (2005). <https://doi.org/10.1117/1.1905343>
34. J. Bonse, P. Rudolph, J. Krüger, S. Baudach, W. Kautek, Appl. Surf. Sci. **154–155**, 659–663 (2000). [https://doi.org/10.1016/S0169-4332\(99\)00481-X](https://doi.org/10.1016/S0169-4332(99)00481-X)
35. G. Miyaji, K. Miyazaki, Opt. Express **16**(20), 16265–16271 (2008). <https://doi.org/10.1364/OE.16.016265>
36. F. Liang, R. Vallée, S.L. Chin, Opt. Mater. Express **2**(7), 1244–1250 (2012). <https://doi.org/10.1364/OME.2.000900>
37. D. Ashkenasi, M. Lorenz, R. Stoian, A. Rosenfeld, Appl. Surf. Sci. **150**(1–4), 101–106 (1999). [https://doi.org/10.1016/S0169-4332\(99\)00228-7](https://doi.org/10.1016/S0169-4332(99)00228-7)
38. A. Rudenko, J.-P. Colombier, S. Höhm, A. Rosenfeld, J. Krüger, J. Bonse, T. Itina, Sci. Rep **7**, 12306 (2017). <https://doi.org/10.1038/s41598-017-12502-4>

Publisher's Note Springer Nature remains neutral with regard to jurisdictional claims in published maps and institutional affiliations.